TULIPs: tunable, light-controlled interacting protein tags for cell biology

Devin Strickland[1], Yuan Lin[2], Elizabeth Wagner[1], C Matthew Hope[1], Josiah Zayner[3], Chloe Antoniou[3], Tobin R Sosnick[3–5], Eric L Weiss[2] & Michael Glotzer[1]

Naturally photoswitchable proteins offer a means of directly manipulating the formation of protein complexes that drive a diversity of cellular processes. We developed tunable light-inducible dimerization tags (TULIPs) based on a synthetic interaction between the LOV2 domain of *Avena sativa* phototropin 1 (AsLOV2) and an engineered PDZ domain (ePDZ). TULIPs can recruit proteins to diverse structures in living yeast and mammalian cells, either globally or with precise spatial control using a steerable laser. The equilibrium binding and kinetic parameters of the interaction are tunable by mutation, making TULIPs readily adaptable to signaling pathways with varying sensitivities and response times. We demonstrate the utility of TULIPs by conferring light sensitivity to functionally distinct components of the yeast mating pathway and by directing the site of cell polarization.

Cells commonly interpret developmental cues through assemblies of structural and signaling proteins that are built up from a combination of transient protein-protein and protein-membrane interactions[1]. These interactions can enforce the proximity of reactant species (for example, a kinase and its substrate) or spatially constrain molecules in the cell to create a polarized response. Designed photoactivatable proteins offer unprecedented spatial and temporal control of cellular signaling processes[2]. For example, a fusion of the small GTPase Rac1 and the photosensor AsLOV2 allows direct control of Rac1 activity in living tissues and has led to ground-breaking experiments on polarity and motility[3–5]. Nevertheless, direct fusion does not always confer photoactivatable control on proteins of interest, even with case-by-case optimization[3].

The ubiquity and modularity of protein-protein and protein-membrane interactions suggests that light-inducible interactions should be an especially flexible tool for triggering cellular signaling events precisely in space and time, thereby obviating the need to optimize the caging of individual proteins. Several groups have adapted light-inducible protein-protein interactions that occur naturally in *Arabidopsis thaliana* for use as cell-biological reagents[6–8]. Whereas each of these methods has attractive features, all have drawbacks. For example, a method based on FKF1 and GIGANTEA requires a large photosensory protein (1,173 amino acids) and has slow association (minutes) and dissociation (hours) kinetics[6]. Another method, based on the large photosensory domain (908 amino acids) of phytochrome B and its interacting factor PIF6, dimerizes within seconds upon illumination with 650-nm light, but recovery requires hours unless dissociation is accelerated by 750-nm light, and precise spatial control requires simultaneous, two-wavelength illumination[7]. A third method, based on cryptochrome 2 and CIB1, features small domains (498 amino acids and 170 amino acids, respectively) that dimerize in 10 s upon illumination and dissociate in 10 min (ref. 8). However, it remains unclear whether the proteins can be used for spatially resolved control of cell signaling[8]. More broadly, the basis of all three light-mediated interactions remains poorly characterized, and the ability to tune important physical parameters is limited.

An ideal light-inducible protein-protein interaction for optogenetics should use small, genetically encoded interacting domains that do not require exogenous cofactors. It should exhibit switching between biologically relevant binding affinities on a range of timescales. Its components should be compatible as fusions to a variety of subcellular markers, and it should be possible to confine photoactivation to a small region of the cell. We set out to create optogenetic dimerization tags with these properties using small, well-characterized interacting domains. We show that the resulting system, TULIPs, is a versatile and tunable optogenetic tool to localize proteins to specific regions of yeast or mammalian cells and to trigger specific cellular-signaling pathways. TULIPs can regulate the activity of nucleotide-exchange factors, scaffold proteins and kinases, all by recruitment to the plasma membrane.

RESULTS

Photoswitch design

As a photosensor, we chose the second light-oxygen-voltage (LOV) domain of *A. sativa* phototropin 1 (AsLOV2)[9]. LOV domains

[1]Department of Molecular Genetics and Cell Biology, The University of Chicago, Chicago, Illinois, USA. [2]Department of Molecular Biosciences, Northwestern University, Evanston, Illinois, USA. [3]Department of Biochemistry and Molecular Biology, The University of Chicago, Chicago, Illinois, USA. [4]Institute for Biophysical Dynamics, The University of Chicago, Chicago, Illinois, USA. [5]Computation Institute, The University of Chicago, Chicago, Illinois, USA. Correspondence should be addressed to M.G. (mglotzer@uchicago.edu).

RECEIVED 2 AUGUST 2011; ACCEPTED 19 JANUARY 2012; PUBLISHED ONLINE 4 MARCH 2012; DOI:10.1038/NMETH.1904

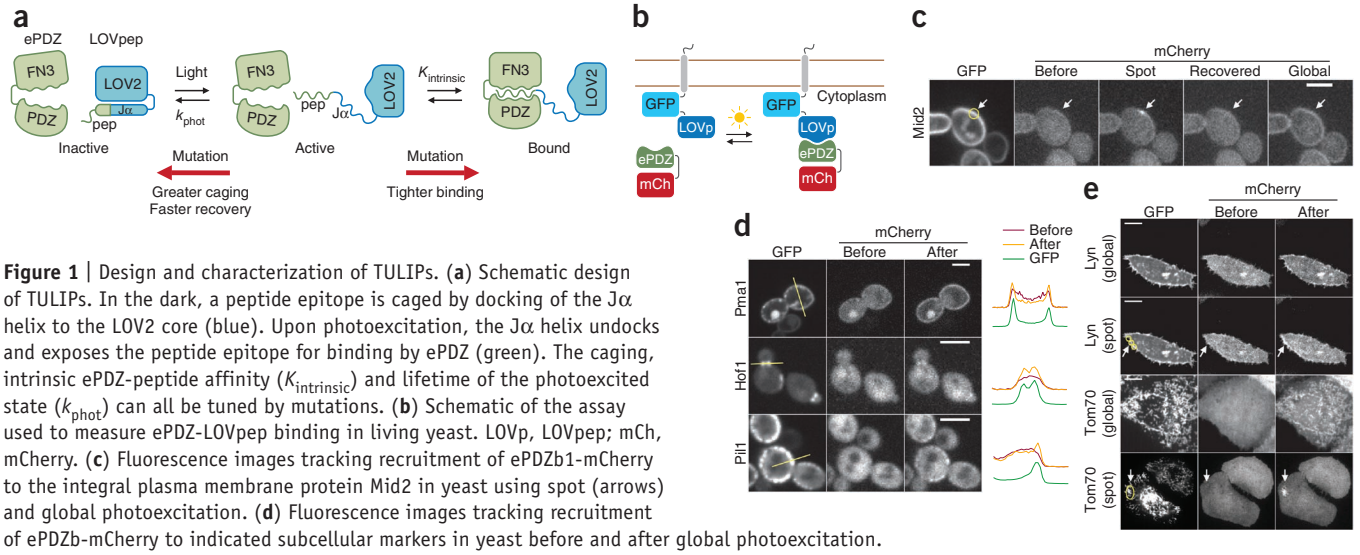

Figure 1 | Design and characterization of TULIPs. (**a**) Schematic design of TULIPs. In the dark, a peptide epitope is caged by docking of the Jα helix to the LOV2 core (blue). Upon photoexcitation, the Jα helix undocks and exposes the peptide epitope for binding by ePDZ (green). The caging, intrinsic ePDZ-peptide affinity ($K_{intrinsic}$) and lifetime of the photoexcited state (k_{phot}) can all be tuned by mutations. (**b**) Schematic of the assay used to measure ePDZ-LOVpep binding in living yeast. LOVp, LOVpep; mCh, mCherry. (**c**) Fluorescence images tracking recruitment of ePDZb1-mCherry to the integral plasma membrane protein Mid2 in yeast using spot (arrows) and global photoexcitation. (**d**) Fluorescence images tracking recruitment of ePDZb-mCherry to indicated subcellular markers in yeast before and after global photoexcitation. The plots depict pixel intensities measured along the yellow lines indicated in the GFP images. (**e**) Fluorescence images tracking recruitment of ePDZb1-mCherry to the plasma membrane and mitochondria of HeLa cells by global and spot (arrows) photoexcitation. Scale bars, 5 μm (**c**,**d**) and 10 μm (**e**).

are small (~125-residue) photosensory domains based on a Per-ARNT-Sim (PAS) core that binds a flavin cofactor. Like many PAS domains, AsLOV2 features flanking N- and C-terminal α helices (the A′α and Jα helices, respectively)[10,11]. Upon photoexcitation with blue light (<500 nm), the Jα helix undocks from the LOV core and unfolds[11,12]. This conformational change is critical to phototropin signaling and has been exploited in designed photosensors[3,13,14]. Many mutational[15–17] and chemical[18] methods of tuning the physical properties of AsLOV2 have been reported.

Following a broadly successful approach for making engineered photoreceptors[19], we reasoned that fusion of a peptide epitope to the C terminus of the Jα helix would allow the LOV2-Jα interaction to sterically block or cage the epitope from binding to a cognate PDZ domain (**Fig. 1a** and **Supplementary Fig. 1**). We anticipated that caging would require sequence overlap so that part of the epitope would adopt a binding-incompetent α-helical conformation in the dark, Jα-docked state[14] (**Supplementary Note 1**). As a binding partner, we used high-affinity, high-specificity engineered variants of the Erbin PDZ domain[20]. These clamshell-like 'ePDZ' chimeras (194 amino acids) are highly tunable; mutational variants of ePDZ and its cognate peptide vary in interaction affinity from ~0.5 nM to >10 μM (ref. 21).

We designed five AsLOV2-peptide fusions for initial screening (**Supplementary Fig. 2a** and **Supplementary Note 1**) by appending a peptide epitope (–SSADTWV–COOH) to serial truncations of the Jα helix. We fused these with GFP (the GFP(S65T) variant) and the transmembrane protein Mid2 and expressed the constructs with monomeric (m)Cherry-tagged ePDZ (**Fig. 1b**). We assayed recruitment of ePDZ-mCherry to the plasma membrane in the dark and immediately after photoexcitation with a 473-nm laser. To quantify the plasma membrane association of ePDZ-mCherry, we measured the ratio of plasma membrane and cytoplasmic fluorescence, averaged over a population of cells ($<R_{obs}>$; **Supplementary Fig. 3** and Online Methods). For the longest AsLOV2-peptide fusions (registers 1–3; **Supplementary Fig. 2a**), $<R_{obs}>$ was relatively high in both the dark and photoexcited states, and photoswitching was slight (**Supplementary Fig. 2b**). Binding was diminished for the shorter fusions (registers 4 and 5; **Supplementary Fig. 2a**), probably because more of the epitope was masked in the Jα-docked conformation. Both constructs exhibited greater binding in the lit state than in the dark, indicating light-directed plasma membrane recruitment of ePDZ-mCherry.

Subcellular recruitment

We modified the register 4 construct to make the sequence more favorable for ePDZ binding and LOV-Jα docking, and named the construct LOVpep (**Supplementary Fig. 2a** and **Supplementary Note 1**). Using this construct, plasma membrane recruitment to Mid2 was reversible on minute timescales and capable of repeated cycles of photoexcitation (**Supplementary Fig. 4**). Using a steerable 440-nm laser to illuminate small (~250 nm) regions, we could reliably and reversibly recruit ePDZb1-mCherry (a high-affinity ePDZ variant fused to mCherry) to a cortical patch (**Fig. 1c**). After localized recruitment, global plasma-membrane recruitment could be stimulated by global photoexcitation (**Fig. 1c**).

We used LOVpep fusions to recruit ePDZb-mCherry (a low-affinity ePDZ variant fused to mCherry) to various subcellular compartments. We tethered GFP-LOVpep to proteins with distinctive localizations, including Hof1 (bud neck), Pil1 (eisosomes) and Pma1 (plasma membrane)[22]. The GFP-LOVpep fusions localized as expected (**Fig. 1d**). ePDZ-mCherry was predominantly cytoplasmic in the dark and localized with GFP-LOVpep upon global photoexcitation.

We also tested TULIPs in cultured HeLa cells. We fused GFP-LOVpep to the plasma membrane localization signal from Lyn kinase[23] and to the mitochondrial outer membrane protein Tom70 (ref. 22), and expressed each of these with ePDZb1-mCherry. In the dark, ePDZb1-mCherry was diffuse in the cytoplasm and nucleoplasm (**Fig. 1e** and **Supplementary Fig. 5**). Upon global blue-light stimulation, ePDZb1-mCherry localized with GFP-LOVpep (**Fig. 1e**). The translocation was reversible for at least three cycles of illumination and recovery (**Supplementary Video 1**). Using spot photoexcitation,

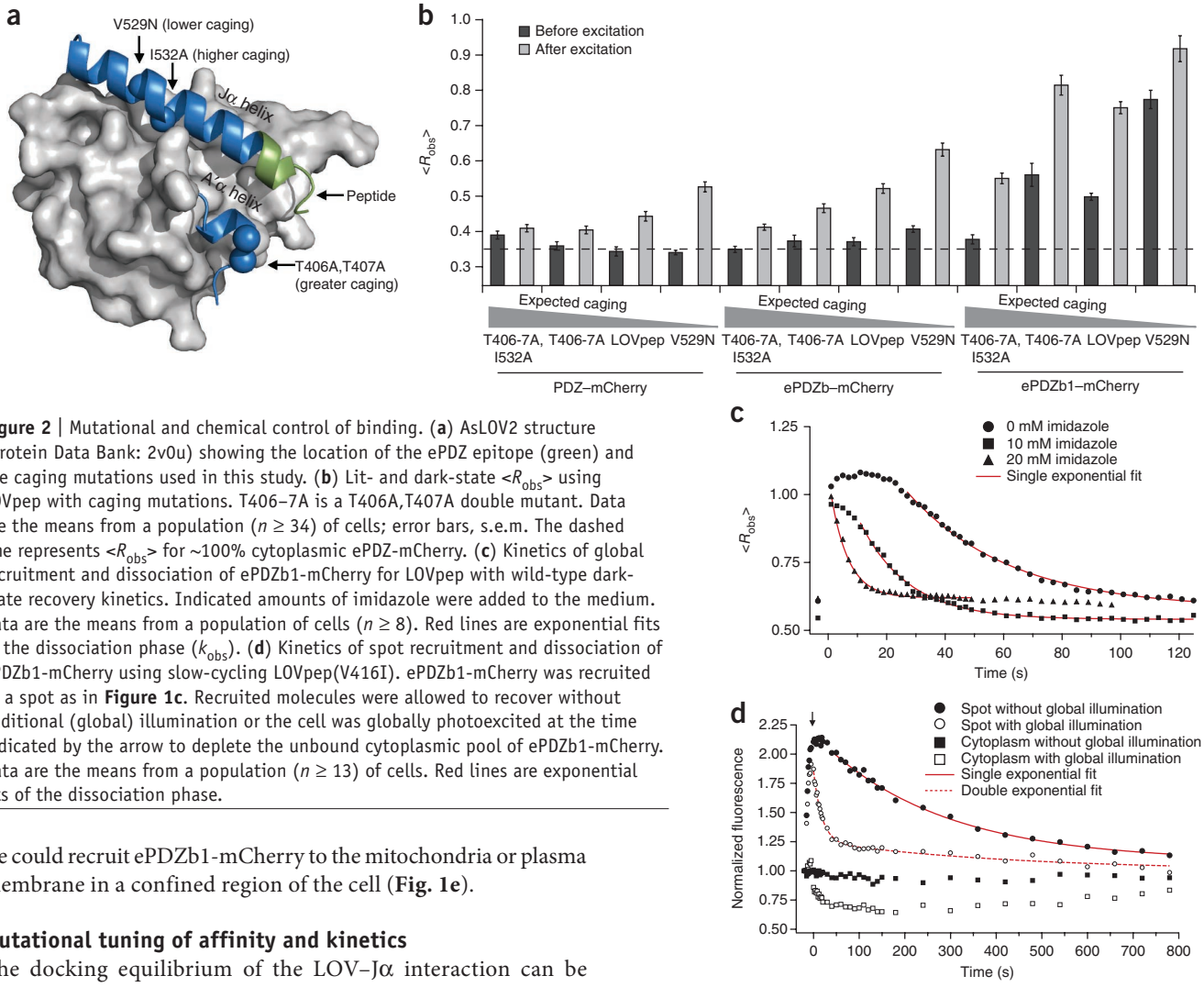

Figure 2 | Mutational and chemical control of binding. (**a**) AsLOV2 structure (Protein Data Bank: 2v0u) showing the location of the ePDZ epitope (green) and the caging mutations used in this study. (**b**) Lit- and dark-state $<R_{obs}>$ using LOVpep with caging mutations. T406–7A is a T406A,T407A double mutant. Data are the means from a population ($n \geq 34$) of cells; error bars, s.e.m. The dashed line represents $<R_{obs}>$ for ~100% cytoplasmic ePDZ-mCherry. (**c**) Kinetics of global recruitment and dissociation of ePDZb1-mCherry for LOVpep with wild-type dark-state recovery kinetics. Indicated amounts of imidazole were added to the medium. Data are the means from a population of cells ($n \geq 8$). Red lines are exponential fits of the dissociation phase (k_{obs}). (**d**) Kinetics of spot recruitment and dissociation of ePDZb1-mCherry using slow-cycling LOVpep(V416I). ePDZb1-mCherry was recruited to a spot as in **Figure 1c**. Recruited molecules were allowed to recover without additional (global) illumination or the cell was globally photoexcited at the time indicated by the arrow to deplete the unbound cytoplasmic pool of ePDZb1-mCherry. Data are the means from a population ($n \geq 13$) of cells. Red lines are exponential fits of the dissociation phase.

we could recruit ePDZb1-mCherry to the mitochondria or plasma membrane in a confined region of the cell (**Fig. 1e**).

Mutational tuning of affinity and kinetics

The docking equilibrium of the LOV–Jα interaction can be changed by mutations, which enables modulation of the dynamic range of effector activity[17]. We tested previously described AsLOV2 mutations that either decrease (V529N[12]) or increase (I532A[17] and T406A,T407A (J.Z., C.A. and T.R.S., unpublished data)) helix docking (**Fig. 2a**). In addition to ePDZb and ePDZb1, we also evaluated recruitment of PDZ-mCherry to explore lower binding affinities. For most recruited proteins, the V529N mutation increased both the lit- and dark-state values of $<R_{obs}>$, indicating increased binding (**Fig. 2b**). In the case of PDZ-mCherry recruitment, dark-state binding was effectively undetectable for LOVpep and the V529N mutant. The T406A,T407A double mutation, which stabilizes the N-terminal A′α helix of AsLOV2 and increases Jα docking affinity, decreased $<R_{obs}>$ for ePDZb-mCherry recruitment, in both the lit and dark states. The T406A,T407A mutation increased $<R_{obs}>$ for ePDZb1-mCherry recruitment (and slightly for dark-state PDZ-mCherry recruitment), perhaps owing to adventitious interactions between the mutated LOV domain and ePDZb1. When paired with ePDZb or ePDZb1, the I532A mutation decreased $<R_{obs}>$ relative to that of the T406A,T407A variant. We also tested mutations in the peptide epitope that have been shown to diminish binding to ePDZ (**Supplementary Note 1** and **Supplementary Fig. 6**). Most previously described mutations in AsLOV2, ePDZ and the peptide epitope exhibited predictable effects on the LOVpep-ePDZ interaction, thereby supporting our design principle (**Fig. 2b** and **Supplementary Fig. 6**). The variants provide a range of experimentally accessible dimerization affinities.

The maximum temporal resolution of experiments using ePDZ-LOVpep depends on the lifetime of the light-recruited complex. When photoexcitation ceases, light-recruited ePDZb fully dissociates from LOVpep within a few minutes *in vivo* (observed rate constant, $k_{obs} = 0.041\ s^{-1}$; **Supplementary Table 1** and **Supplementary Video 2**). We investigated whether this observed dark-state dissociation rate (k_{obs}) follows the LOVpep dark-state recovery rate (k_{phot}) or the intrinsic ePDZ-peptide dissociation rate (k_{diss}). The rate k_{diss} is slower for ePDZb1 than for ePDZb when binding to model peptide substrates *in vitro* (~10^{-4} s^{-1} and ~10^{-2} s^{-1}, respectively)[20]. However k_{obs} was remarkably similar for ePDZb-mCherry and ePDZb1-mCherry (**Supplementary Table 1** and **Supplementary Video 2**). Using a mutated LOVpep(V416I) with approximately tenfold slower dark-state recovery[16], k_{obs} was again similar for the ePDZb-mCherry and ePDZb1-mCherry, and both rates were similar to the slower k_{phot} (**Supplementary Table 1**). To test whether k_{obs} can be increased, we chemically accelerated k_{phot} by adding imidazole to the medium[18]. As with mutational tuning, changes in k_{obs} generally tracked changes in k_{phot} (**Fig. 2c** and

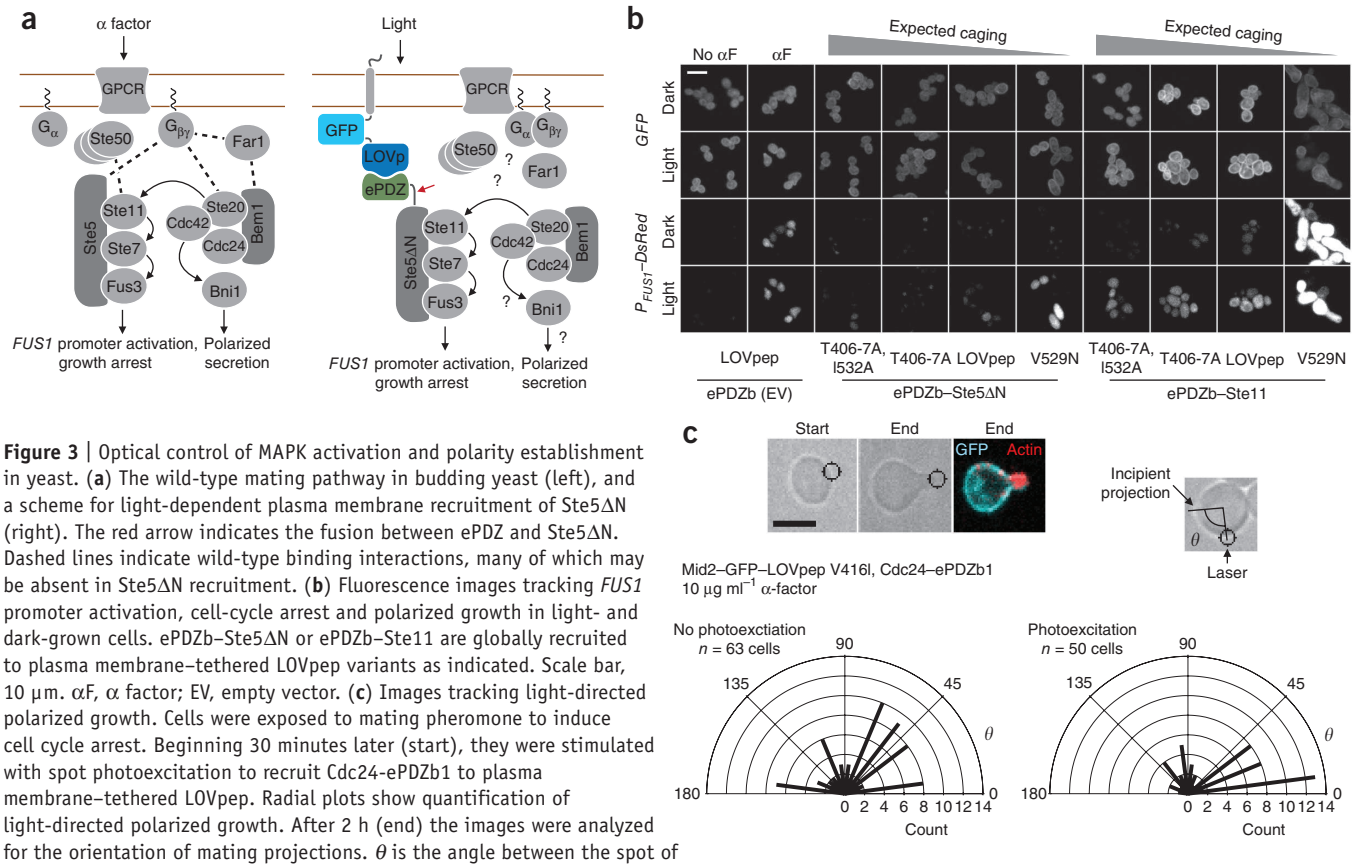

Figure 3 | Optical control of MAPK activation and polarity establishment in yeast. (**a**) The wild-type mating pathway in budding yeast (left), and a scheme for light-dependent plasma membrane recruitment of Ste5ΔN (right). The red arrow indicates the fusion between ePDZ and Ste5ΔN. Dashed lines indicate wild-type binding interactions, many of which may be absent in Ste5ΔN recruitment. (**b**) Fluorescence images tracking *FUS1* promoter activation, cell-cycle arrest and polarized growth in light- and dark-grown cells. ePDZb–Ste5ΔN or ePDZb–Ste11 are globally recruited to plasma membrane–tethered LOVpep variants as indicated. Scale bar, 10 μm. αF, α factor; EV, empty vector. (**c**) Images tracking light-directed polarized growth. Cells were exposed to mating pheromone to induce cell cycle arrest. Beginning 30 minutes later (start), they were stimulated with spot photoexcitation to recruit Cdc24-ePDZb1 to plasma membrane–tethered LOVpep. Radial plots show quantification of light-directed polarized growth. After 2 h (end) the images were analyzed for the orientation of mating projections. θ is the angle between the spot of laser photoexcitation, the center of the cell and the incipient projection (top right). Radial bars depict the number of polarization events of angle θ in each 15° sector. 'No photoexcitation' denotes a negative control experiment in which the spot photoexcitation laser was switched off. $P < 0.01$ for a comparison of experimental and control distributions (two-sample Kolmogorov-Smirnov). Scale bar, 5 μm.

Supplementary Table 1). Taken together, the data indicate that mutational or chemical modulation of the dark-state recovery of LOVpep also controls k_{obs}.

These data are compatible with two models: either the ePDZ-LOVpep complex persists as long as the lit state, or the bound ePDZ rapidly exchanges with the unbound pool. To distinguish between these, we observed ePDZ-mCherry dissociation from a locally photoexcited spot. Spot recruitment did not deplete the unbound pool; therefore the LOVpep occupancy was higher than during global recruitment (**Fig. 1c**). The dissociation of spot-recruited ePDZ-mCherry followed single-exponential kinetics with a rate similar to k_{phot} when left unperturbed but followed biphasic kinetics when the cytoplasmic pool was rapidly depleted by global photoexcitation after a few seconds (**Fig. 2d**, **Supplementary Table 2** and **Supplementary Video 3**). Most of the bound ePDZ-mCherry dissociated quickly, but the remainder dissociated slowly with a rate matching k_{obs} and k_{phot}. Taken together, the data suggest that bound ePDZ rapidly exchanged with the unbound pool. When the unbound pool was quickly depleted by global recruitment, the amount of spot-recruited ePDZ was above the new equilibrium value. Re-equilibration occurred with the rapid dissociation of ePDZ, whereas the equilibrium itself changed slowly as the LOVpep reverted to the low-affinity dark state with the rate k_{phot}. Fast dissociation kinetics and a continuously tunable photoexcitation lifetime are potentially desirable features for an optogenetic tool because together they allow precise temporal control in biological experiments.

Optical control of MAPK activation and polarity

We asked whether TULIPs can be used for light-activated cellular signaling. The yeast mating pathway normally is initiated by binding of a peptide pheromone to a G protein–coupled receptor (GPCR) (**Fig. 3a**). Downstream, components of two conserved signaling modules are recruited to the plasma membrane by the activated G protein: one comprising a mitogen activated protein kinase (MAPK) cascade organized by the scaffold Ste5 and the other comprising the GTPase Cdc42 and its associated scaffolds, guanine nucleotide exchange factor and effectors. The MAPK module, whose activation leads to G1 arrest and transcription of mating-specific genes, has been extensively engineered in attempts to elucidate its workings[24]. Notably, tethering Ste5 or Ste11 to the plasma membrane robustly activates the pathway[25,26]. The Cdc42 module is required for polarized growth in budding yeast, and its activation is usually constrained by intrinsic or extrinsic spatial cues[27]. Disruption of Cdc42-mediated polarization in vegetatively growing cells prevents budding, but not isotropic growth, and leads to an enlarged terminal phenotype[27].

We screened a variety of MAPK- and Cdc42-associated proteins for growth defects upon plasma-membrane recruitment. We performed initial experiments with a constitutively active LOVpep variant ($LOVpep^{CA}$) fused to Mid2 and under control of the galactose-inducible *GAL1* promoter. Several proteins, when fused to ePDZb caused growth arrest upon galactose-induced expression of $LOVpep^{CA}$ (**Supplementary Fig. 7**).

We next asked whether light-dependent recruitment of ePDZb-Ste5ΔN (Ste5ΔN is a truncated protein deficient in G-protein binding[25]) and ePDZb-Ste11 could cause MAPK pathway activation (**Fig. 3a**). There was little or no detectable dark-state growth arrest upon galactose induction over a range of expected affinities (**Supplementary Fig. 8**), indicating that the ePDZb-LOVpep interaction is well caged in the dark with respect to biological activity. However, continuous illumination caused growth arrest in some strains and the extent of arrest corresponded with the expected affinity of the LOVpep variant (**Supplementary Fig. 8**).

To characterize the phenotype, we illuminated cells for 4 h in liquid culture and then examined them by microscopy and flow cytometry. As expected, αF-stimulated control cells formed mating projections (shmoos) and transcribed a *FUS1* promoter–driven *DsRed-Max* reporter gene[28]; these cells also did not show light-stimulated pathway activation (**Fig. 3b** and **Supplementary Fig. 9**). For ePDZb-Ste5ΔN recruitment, highly caged LOVpep variants did not measurably activate the pathway (**Fig. 3b** and **Supplementary Fig. 9**). This level of dark-state suppression is consistent with our previous observation that strong Jα docking can suppress effector activity even under full photoexcitation[17]. In contrast, less strongly caged LOVpep variants allowed more robust light-dependent cell-cycle arrest and polarized growth, presumably because the weaker peptide caging leads to greater Ste5ΔN recruitment. Conversely, more caging was required to bring ePDZb-Ste11 recruitment into a sensitive range, with the less caged variants causing constitutive activation (**Fig. 3b** and **Supplementary Fig. 9**). Light-stimulated cells were less polarized than αF-stimulated cells, even though both had stopped forming buds (**Fig. 3b**).

To determine whether TULIPs can also control GTPase signaling pathways, we examined light-directed recruitment of Cdc24-ePDZb1 to Mid2-GFP-LOVpep. Global recruitment caused a growth arrest with a terminal phenotype of large, round cells that depended on the strength of the ePDZ–peptide interaction (**Supplementary Fig. 10**). The ability of full-length Cdc24 to block polarization upon global recruitment was surprising as earlier work indicated that the protein was autoinhibited[29]. This discrepancy could result from the efficiency with which the protein was recruited (**Supplementary Fig. 10**).

To determine whether plasma membrane–localized Cdc24 is active, we locally recruited Cdc24-ePDZb1 to specify the direction of polarized growth. Indeed, we could specify the orientation of mating projection growth in αF-arrested cells (**Fig. 3c** and **Supplementary Video 4**), suggesting that the GEF was intrinsically active. This result demonstrated that the TULIPs system can be used to control the activity of signaling molecules with high spatial precision, even in small (~5 μm diameter) cells.

DISCUSSION

Our approach, though conceptually similar to other strategies based on light-directed recruitment[6–8], offers unique advantages. First, both components are small, facilitating genetic manipulation, and do not require an exogenous cofactor[6]. Second, both proteins are structurally and biophysically well-characterized. The mechanism by which AsLOV2 modulates the activity of heterologous effectors is generally well-understood[3,11,12,17], and our findings indicate that these principles are applicable to the ePDZ-LOVpep interaction. Variants with many tuning mutations, including alterations of the intrinsic affinity, the stability of Jα helix docking and the photocycle time, are available and can be easily incorporated into experiments (Online Methods and **Supplementary Note 2**). In principle, many activation mechanisms should be light-controllable using TULIPs, such as transcriptional regulation, enzyme-substrate enforced proximity and protein-fragment complementation.

Even in simple engineered systems, small changes in binding affinity can greatly impact function[30]. A failed or suboptimal implementation can be due to either design flaws or a poor choice of a parameter value, yet it is usually not obvious a priori which parameter values will be best. Just as electronics prototyping requires a ready assortment of resistors, capacitors and transistors with different characteristics, our experiments demonstrate that biological prototyping requires protein modules that are quantifiably tunable to ensure robust activation of a pathway of interest.

METHODS

Methods and any associated references are available in the online version of the paper at http://www.nature.com/naturemethods/.

Note: Supplementary information is available on the Nature Methods website.

ACKNOWLEDGMENTS

We thank B. Glick (University of Chicago), S. Koide (University of Chicago) and F. Cross (Rockefeller University) for sharing plasmids, and members of the Glotzer, Weiss, Sosnick, Munro, Kovar and Glick laboratories for helpful discussions. This work was supported by research (GM088668, M.G. and T.R.S.) and training grants from the US National Institutes of Health, a grant from the Chicago Biomedical Consortium with support from the Searle Funds at the Chicago Community Trust (M.G., T.R.S. and E.L.W.), and by an American Cancer Society Postdoctoral Fellowship to D.S. (119248-PF-10-134-01-CCG).

AUTHOR CONTRIBUTIONS

D.S. and M.G. conceived of the TULIPs strategy. D.S., Y.L., E.W., E.L.W. and M.G. designed experiments. D.S., Y.L., E.W. and C.M.H. performed experiments. D.S., Y.L., E.W., C.M.H., T.R.S., E.L.W. and M.G. analyzed data. J.Z., C.A. and T.R.S. provided new AsLOV2 mutations. D.S., E.L.W. and M.G. wrote the paper.

COMPETING FINANCIAL INTERESTS

The authors declare competing financial interests: details accompany the full-text HTML version of the paper at http://www.nature.com/naturemethods/.

Published online at http://www.nature.com/naturemethods/.
Reprints and permissions information is available online at http://www.nature.com/reprints/index.html.

1. Hartman, N.C. & Groves, J.T. Signaling clusters in the cell membrane. *Curr. Opin. Cell Biol.* **23**, 370–376 (2011).
2. Toettcher, J.E., Voigt, C.A., Weiner, O.D. & Lim, W.A. The promise of optogenetics in cell biology: interrogating molecular circuits in space and time. *Nat. Methods* **8**, 35–38 (2011).
3. Wu, Y.I. *et al.* A genetically encoded photoactivatable Rac controls the motility of living cells. *Nature* **461**, 104–108 (2009).
4. Yoo, S.K. *et al.* Differential regulation of protrusion and polarity by PI3K during neutrophil motility in live zebrafish. *Dev. Cell* **18**, 226–236 (2010).
5. Wang, X., He, L., Wu, Y.I., Hahn, K.M. & Montell, D.J. Light-mediated activation reveals a key role for Rac in collective guidance of cell movement *in vivo*. *Nat. Cell Biol.* **12**, 591–597 (2010).
6. Yazawa, M., Sadaghiani, A.M., Hsueh, B. & Dolmetsch, R.E. Induction of protein-protein interactions in live cells using light. *Nat. Biotechnol.* **27**, 941–945 (2009).
7. Levskaya, A., Weiner, O.D., Lim, W.A. & Voigt, C.A. Spatiotemporal control of cell signalling using a light-switchable protein interaction. *Nature* **461**, 997–1001 (2009).
8. Kennedy, M.J. *et al.* Rapid blue-light-mediated induction of protein interactions in living cells. *Nat. Methods* **7**, 973–975 (2010).
9. Christie, J.M. *et al. Arabidopsis* NPH1: a flavoprotein with the properties of a photoreceptor for phototropism. *Science* **282**, 1698–1701 (1998).

10. Halavaty, A.S. & Moffat, K. N- and C-terminal flanking regions modulate light-induced signal transduction in the LOV2 domain of the blue light sensor phototropin 1 from *Avena sativa*. *Biochemistry* **46**, 14001–14009 (2007).
11. Harper, S.M., Neil, L.C. & Gardner, K.H. Structural basis of a phototropin light switch. *Science* **301**, 1541–1544 (2003).
12. Yao, X., Rosen, M.K. & Gardner, K.H. Estimation of the available free energy in a LOV2-J alpha photoswitch. *Nat. Chem. Biol.* **4**, 491–497 (2008).
13. Harper, S.M., Christie, J.M. & Gardner, K.H. Disruption of the LOV-Jalpha helix interaction activates phototropin kinase activity. *Biochemistry* **43**, 16184–16192 (2004).
14. Strickland, D., Moffat, K. & Sosnick, T.R. Light-activated DNA binding in a designed allosteric protein. *Proc. Natl. Acad. Sci. USA* **105**, 10709–10714 (2008).
15. Christie, J.M. *et al.* Steric interactions stabilize the signaling state of the LOV2 domain of phototropin 1. *Biochemistry* **46**, 9310–9319 (2007).
16. Zoltowski, B.D., Vaccaro, B. & Crane, B.R. Mechanism-based tuning of a LOV domain photoreceptor. *Nat. Chem. Biol.* **5**, 827–834 (2009).
17. Strickland, D. *et al.* Rationally improving LOV domain-based photoswitches. *Nat. Methods* **7**, 623–626 (2010).
18. Alexandre, M.T., Arents, J.C., van Grondelle, R., Hellingwerf, K.J. & Kennis, J.T. A base-catalyzed mechanism for dark state recovery in the Avena sativa phototropin-1 LOV2 domain. *Biochemistry* **46**, 3129–3137 (2007).
19. Möglich, A. & Moffat, K. Engineered photoreceptors as novel optogenetic tools. *Photochem. Photobiol. Sci.* **9**, 1286–1300 (2010).
20. Huang, J., Koide, A., Makabe, K. & Koide, S. Design of protein function leaps by directed domain interface evolution. *Proc. Natl. Acad. Sci. USA* **105**, 6578–6583 (2008).
21. Huang, J., Makabe, K., Biancalana, M., Koide, A. & Koide, S. Structural basis for exquisite specificity of affinity clamps, synthetic binding proteins generated through directed domain-interface evolution. *J. Mol. Biol.* **392**, 1221–1231 (2009).
22. Huh, W.K. *et al.* Global analysis of protein localization in budding yeast. *Nature* **425**, 686–691 (2003).
23. Inoue, T., Heo, W.D., Grimley, J.S., Wandless, T.J. & Meyer, T. An inducible translocation strategy to rapidly activate and inhibit small GTPase signaling pathways. *Nat. Methods* **2**, 415–418 (2005).
24. Pryciak, P.M. Designing new cellular signaling pathways. *Chem. Biol.* **16**, 249–254 (2009).
25. Pryciak, P.M. & Huntress, F.A. Membrane recruitment of the kinase cascade scaffold protein Ste5 by the Gβγ complex underlies activation of the yeast pheromone response pathway. *Genes Dev.* **12**, 2684–2697 (1998).
26. Winters, M.J., Lamson, R.E., Nakanishi, H., Neiman, A.M. & Pryciak, P.M. A membrane binding domain in the ste5 scaffold synergizes with Gβγ binding to control localization and signaling in pheromone response. *Mol. Cell* **20**, 21–32 (2005).
27. Park, H.O. & Bi, E. Central roles of small GTPases in the development of cell polarity in yeast and beyond. *Microbiol. Mol. Biol. Rev.* **71**, 48–96 (2007).
28. Strack, R.L. *et al.* A noncytotoxic DsRed variant for whole-cell labeling. *Nat. Methods* **5**, 955–957 (2008).
29. Shimada, Y., Wiget, P., Gulli, M.P., Bi, E. & Peter, M. The nucleotide exchange factor Cdc24p may be regulated by auto-inhibition. *EMBO J.* **23**, 1051–1062 (2004).
30. Dueber, J.E., Yeh, B.J., Chak, K. & Lim, W.A. Reprogramming control of an allosteric signaling switch through modular recombination. *Science* **301**, 1904–1908 (2003).

ONLINE METHODS

Plasmid and strain construction. S. Koide (University of Chicago) provided plasmids encoding ePDZ variants. B. Glick (University of Chicago) provided plasmids encoding PMA1 and DsRedMax. F. Cross (Rockefeller University) provided a plasmid encoding the Gal4-rMR construct. All ARS CEN plasmids used in this study were from the pGREG series[31]. All integrating plasmids were of the YIplac series[32]. The *MET25*, *TEF* and *ADH* promoters were from the PCR Toolbox plasmids[33]. All other yeast coding sequences were obtained by PCR from the Yeast Genomic Tiling Collection (Open Biosystems) or from genomic DNA.

DNA manipulations were simulated with a prerelease version of the SnapGene software (GSL Biotech). Plasmids were generated using a combination of conventional ligation, InFusion cloning (Clontech) and recombination in yeast[31]. Yeast were transformed using lithium acetate, single-stranded carrier DNA and polyethylene glycol[34]. All plasmids and strains were verified by colony PCR or DNA sequencing.

We constructed the background strain YLS1254 by integrating a *Gal4-rMR* expression cassette[35] into W303 *MAT***a** so as to delete the endogenous *TRP1* coding sequence using a *URA3* marker, which was itself subsequently deleted[36]. We then integrated a sequence encoding C-terminal mCherry tag at the endogenous *ABP1* coding sequence using a *HIS3MX* marker[37].

TULIPs plasmid system. We deposited a set of plasmids for the TULIPs system, along with maps and sequences, in Addgene (**Supplementary Tables 3** and **4**). The plasmids allow cloning of protein coding sequences with GFP-LOVpep, cpPDZ, ePDZb and ePDZb1 as tags. We have provided integrating versions, based on the YIplac series of plasmids, and centromeric versions, based on the pGREG series of plasmids.

Our cloning scheme is based on *in vitro* recombination cloning such as the InFusion system (Clontech), or a previously published method[38]. Cloning by recombination in yeast can also be used with the centromeric plasmids[31]. See **Supplementary Table 5** for primer details.

Affinity, caging and switching. We use the term 'intrinsic affinity' to denote the intrinsic affinity of binding between a photoactivated, helix-undocked LOVpep and free ePDZ (**Supplementary Fig. 1**). We use the term 'caging' for the diminishment of LOVpep-ePDZ binding in the dark state. Quantitatively this is the ratio of the dark-state dissociation constant to the intrinsic dissociation constant. We use the term 'switching' to refer to the ratio of the dark- and lit-state dissociation constants. Because it is possible for a highly stabilized helix to remain substantially docked to the LOV core even in the lit state, caging and switching may have different values. However, caging is always numerically greater than or equal to switching. We use the term 'overall affinity' to refer to the observed affinity of the reaction scheme depicted in **Figure 1a**.

Plasma membrane recruitment assay. We used a plasma-membrane recruitment assay in living yeast to assess the lit- and dark-state binding between ePDZ and the LOV–peptide fusions. We fused GFP–AsLOV2–peptide constructs to the C terminus of the integral plasma membrane protein Mid2 (ref. 22). We expressed the P_{TEF}*–Mid2–GFP–LOVpep* constructs from ARS/CEN plasmids maintained with a *LEU2* or *KanMX* marker. Generally, GFP fluorescence was cleanly and evenly localized to the plasma membrane and accumulation in endocytic compartments was minimal. Sometimes GFP fluorescence was also localized to the vacuole or nuclear periphery, but this was always less intense than the plasma membrane signal and did not interfere with image thresholding.

We expressed the LOV-peptide constructs together with mCherry-tagged ePDZ (**Fig. 1b**). To ensure that binding affinity was in a sensitive range for the assay, we used moderate- and high-affinity ePDZ variants (ePDZb and ePDZb1, respectively, having a tenfold difference in affinity for model peptides)[20]. We expressed P_{TEF}*-ePDZ–mCherry* or P_{TEF}*-PDZ–mCherry* constructs from a plasmid integrated at the *URA3* locus. This combination of ARS/CEN and integrating plasmids provided the most consistent expression as judged by GFP and mCherry fluorescence. Diploid JK9-3d strains harboring both plasmids were constructed by mating singly transformed haploids and selecting on synthetic dropout (SD) medium without leucine or uracil (SD–Leu –Ura).

We grew cells in liquid yeast extract, peptone and dextrose (YPD) medium with G418, then pelleted and resuspended the cells in minimal medium. We plated 3 µl of the cell suspension on a 2 × 2 × 0.1 cm, 1.2% agar pad made with the same medium. We then placed a #1.5 coverslip over the pad and sealed the edges with petroleum jelly[39]. We imaged the cells on an Axiovert 200M microscope (Zeiss) equipped with a spinning disk confocal (CSU10, Yokogawa) and an electron-multiplying charge-coupled device (EMCCD) camera (Cascade 512B, Photometrics) using a 63×, 1.4 numerical aperture (NA) objective. The microscope was controlled using MetaMorph (Molecular Devices). We placed a 550-nm long-pass filter (Edmund Optics) in the transmitted light path to avoid photoexciting the LOV domain when using phase contrast.

We assayed recruitment of ePDZ-mCherry to the plasma membrane in the dark and immediately after photoexcitation with a 473-nm laser. To quantify the plasma membrane association of ePDZ-mCherry, we measured the ratio of plasma membrane and cytoplasmic fluorescence, averaged over a population of cells ($<R_{obs}>$, see below and **Supplementary Fig. 3**). We used an ImageJ macro to quantify recruitment with minimal user intervention. Because the algorithm works best with individual cells or mother-daughter pairs that are well-separated from other cells, we searched for fields of well-separated cells using Nomarski illumination. We then took a 500-ms image of mCherry fluorescence and a 125-ms image of GFP fluorescence. We used an additional 1-s pulse (473 nm) to ensure the LOV domain was fully photoexcited (see below). For basic recruitment assays, we took a single 500-ms image of mCherry fluorescence after a 1–10 s delay to allow recruitment to reach the maximum level. For kinetic assays, we acquired a time lapse of 500-ms images.

Quantification included the following steps: first, a stack registration plugin (StackReg[40]) corrected for stage drift. This was especially important for long time-lapse imaging in kinetic assays. Second, a thresholding method automatically defined regions of interest (ROIs) for the plasma membrane, cytoplasm and background based on the GFP image (**Supplementary Fig. 3a**). There was no user intervention in defining the ROIs, but cells that were not thresholded accurately (for example, because of nearby dust particles) were discarded. Third, for each frame of

a given cell the average, background-subtracted intensities were measured in the plasma membrane, cytoplasm ROIs. The ratio of the plasma membrane and cytoplasm intensities (R_{obs}) were also calculated. Notably, the background autofluorescence of the medium and the cellular mCherry fluorescence have different photobleaching properties. Because R_{obs} is a ratio of two background-subtracted values it is somewhat sensitive to this difference, and this sensitivity is especially apparent when photoexciting over multiple cycles. However, we have not attempted to correct for this phenomenon in any assays. We collated the data and calculated the mean, denoted $<R_{obs}>$, and standard error for populations of cells using Excel (Microsoft), and plotted the data using Igor Pro (Wavemetrics).

Interpretation of $<R_{obs}>$. Empirically, $<R_{obs}>$ ranged from ~0.35 to ~2.5. We estimated the lower value by globally evaluating multiple datasets. We found that $<R_{obs}>$ was never less than ~0.30, and all data approached a value of ~0.35 as the expected affinity decreased. We confirmed the assignment of ~0.35 as 100% cytoplasmic fluorescence by inspecting a subset of cells with individual R_{obs} of 0.34–0.36. mCherry fluorescence was strongly cytoplasmic in these cells (**Supplementary Fig. 3b**). In **Figure 2** and **Supplementary Figure 2b**, we indicate that $<R_{obs}> = 0.35$ is estimated to be 100% cytoplasmic. In **Supplementary Figure 6**, the lowest observed $<R_{obs}>$ was ~0.30, and we adjusted the 100% cytoplasmic estimate to this lower value. Although not ideal, this adjustment is needed because of a small amount of systematic variation in $<R_{obs}>$ seen across experiments (data not shown).

We designed our thresholding algorithm to analyze large and variable populations of cells quickly and with minimal user intervention. In choosing an automated thresholding algorithm we favored robustness and a high signal-to-noise ratio. However, this robustness comes at the expense of capturing the true extremes of plasma membrane and cytoplasmic fluorescence, and the method tends to compress the numerical range of $<R_{obs}>$. Furthermore, a given $<R_{obs}>$ value should not be interpreted as representing a clearly defined ratio of bound and unbound molecules. For example, $<R_{obs}> = 1$ should not be taken to mean that 50% of the molecules are plasma membrane–bound and 50% are cytoplasmic.

Global illumination during live-cell microscopy. We used the same 473-nm laser as for GFP imaging. The light intensity measured at the back of the objective was 750 μJ s^{-1}. Using the conservative assumption that all of this light was evenly distributed across the area imaged by the camera (1.23×10^{-4} cm^2), the irradiance was 6.1 J cm^{-2} s^{-1}. We generally used 1.125 s total blue light photoexcitation (6.9 J cm^{-2}) for ePDZ–mCherry recruitment assays. For comparison, a recent study examining the effects of phototoxicity in budding yeast[41] used 4-s blue-light pulses of 4.9 J cm^{-2} every 20 s for GFP image acquisition (that is, in addition to constant illumination used as the experimental source of phototoxicity). Imaging illumination itself was well below the apparent threshold for a detectable stress response in their experiments[41].

We assessed whether lower levels of illumination could elicit ePDZ-mCherry recruitment. We clearly detected recruitment after a 0.063 s pulse with a 10% transmission filter in the excitation path (0.038 J cm^{-2}, **Supplementary Fig. 10a**). This is considerably less power than would be used for routine GFP imaging.

Spot illumination. We used a galvanometer-steerable 440-nm dye laser (Micropoint, Photonics Instruments) to locally photoexcite Mid2-localized LOVpep. We controlled the illumination intensity using an adjustable internal attenuator plate and an external optical density of 1.0 absorptive neutral density filter (Thor Labs) placed in the beam path.

We did not measure the Micropoint laser intensity directly. However, with the attenuator plate set to ~30% transmission, three pulses of the laser were just sufficient to ablate the reflective coating on the calibration slide provided with the instrument. We used this setting as the reference power for experiments. Five pulses at the reference power were sufficient to slightly bleach Mid2-GFP (**Supplementary Fig. 10b**). After five pulses at 10–11% of the reference power (attenuated with either the attenuator plate or the external filter), Mid2-GFP bleaching was nearly undetectable. For spot photoexcitation experiments we used five pulses at ~1% of the reference power (that is, with the attenuator set at 3% and the external filter in place). Five pulses at this power were more effective than a single higher-power pulse for spot recruitment.

Spot photoexcitation kinetics. We manually defined ROIs corresponding to the recruited spot, cytoplasm and background, and measured the average pixel intensities for these regions over all time points. We fit background-subtracted spot intensities to one- and two-exponential functions using IgorPro. For the spot-only experiments, a two-exponential function did not offer any improvement over a one-exponential function. For the spot plus global experiments both datasets were better approximated by a two-exponential function (data not shown). Nevertheless, we provided the rate constant for the one-exponential fit for wild-type cycling LOVpep (**Supplementary Table 2**).

HeLa culture and transfection. We grew HeLa cells in Dulbecco's modified Eagle medium (DMEM) supplemented with 10% FBS, 100 U penicillin and 0.1 mg ml^{-1} streptomycin at 37 °C in 5% CO_2. We transfected cells using Lipofectamine 2000 (Invitrogen) according to standard protocols. We grew cells overnight on glass coverslips and transfected them with 0.5–1 μg of plasmid DNA the next day. The following day, we transferred the cells to phenol-free DMEM, laid the coverslips directly on a microscope slide and sealed the edges with petroleum jelly.

For the Lyn and Tom70 global recruitment experiments, we used LOVpep with the lysine at position –6 mutated to arginine and the threonine at position –2 mutated to serine (where 0 is the C-terminal amino acid, **Supplementary Fig. 2a**). For the Tom70 spot recruitment experiments, we used LOVpep(T406A, T407A,I532A). The choice of the first allele was arbitrary, and we have no reason to expect that any of the mutations are optimal for mammalian cells. Indeed, we found the more highly caged T406A,T407A,I532A variant superior in the Tom70 spot recruitment experiment. We performed global and spot recruitment assays essentially as described for yeast.

Blue LED illumination. Blue AlGaInP LEDs (http://www.theledlight.com/, 20° viewing angle, 8,000 millicandela, 468-nm λmax at 3.4 V) were arranged into 6 × 8 arrays by pressing into an empty pipet tip rack and soldered together in parallel. The entire array was powered with a 3.3 V, 1.2 A power supply (Phihong PSA05R-033).

doi:10.1038/nmeth.1904

The unfiltered light intensity from the LED arrays was ~0.005 J cm^{-2} s^{-1}. A considerably higher intensity (>0.037 J cm^{-2} s^{-1}) was required to elicit nuclear shuttling of the transcription factor Msn2, an indicator of environmental stress in budding yeast[41]. For MAPK activation and polarity-disruption experiments, we attenuated the light intensity with either colored plastic notebook dividers (Avery) or transparency sheets laser-printed with a uniform gray tone. In either case, we determined the transmission at 465 nm using spectroscopy. In these experiments, 10% of the raw LED intensity was sufficient to elicit a strong biological response.

Growth arrest assay. For all signaling assays, we used a modified Mid2 construct, Mid2(SS/TM), containing only the signal sequence and transmembrane helix. To assay growth arrest on solid medium, we made 1:10 serial dilutions of cells (grown in liquid culture or resuspended from plates) in water. We spotted the dilutions onto yeast extract and peptone (YP) medium with 2% dextrose or 2% galactose, with G418 to maintain CEN plasmids. We grew the plates at room temperature, either foil-wrapped for dark plates or under an LED array with filters for 10% transmission for lit plates. We wrapped the edges of the plates with Parafilm to prevent drying and kept the plates with the growth surface facing down. For lit plates, we positioned fans to blow across the plates to dissipate heating from the LED array and placed the plates on a foil surface to reflect transmitted light back onto the growth surface.

Assay for light-dependent mating pathway activation. We grew overnight cultures (YLS2067 background with plasmids as indicated) in 5 ml YP with 2% galactose and G418. If the overnight cultures were above OD_{600} = 0.8, then we diluted the cultures with the same medium to OD_{600} = 0.2 and grew them for an additional 2 h. We diluted the log-phase cultures to OD_{600} = 0.1 to 0.2 and aliquoted 100 µl into standard clear 96-well microtiter plates. For alpha-factor stimulation, we added 5 µl medium with 20× alpha factor.

We incubated the cultures at room temperature with shaking for 4 h. Dark plates were foil-wrapped, and lit plates were under an LED array with filters for 10% transmission.

For microscopy, we spun down 50–100 µl and resuspended them in 5–10 µl SC. We spotted 2 µl onto 10 mm × 10 mm × 1 mm thick agarose pad made with SC (four pads per slide) and sealed the edges with vaseline[39]. We imaged with a 40× objective (Zeiss).

For flow cytometry, we pelleted the cells and resuspended in phosphate buffered saline. We collected DsRedMax[28] fluorescence intensities on a BD Biosciences LSR II flow cytometer using a 561 nm excitation laser and a 610 nm ± 20 nm emission filter, and analyzed the data using FlowJo (Tree Star).

Assay for light-dependent polarity disruption. We grew overnight cultures (YLS1254 background with plasmids as indicated) in 5 ml YP with 2% galactose. We aliquoted 100 µl into standard clear 96-well microtiter plates and incubated them at room temperature with shaking for 5 h. Dark plates were foil-wrapped, and lit plates were under an LED array with filters for 10% transmission.

For microscopy, we spun down 50–100 µl and resuspended in 5–10 µl SC. We spotted 2 µl onto 10 mm × 10 mm × 1 mm thick agarose pad made with SC (four pads per slide), placed a coverslip on the pad and sealed the edges with Vaseline. We imaged with a 40× objective.

Assay for light-dependent polarity specification. We grew overnight cultures (YLS2446) in SC without His, Leu –Met –Ura with 2× adenine with 20 µM deoxycorticosterone (DOC[35]) in foil-wrapped tubes. We spun down 1–1.5 ml of the overnight culture and resuspended in 20 µl of the same medium with 10 µM DOC and 10 µg ml^{-1} α factor (αF), and incubated this in the dark for 30 min. We spotted 2 µl of this suspension onto 10 mm × 10 mm × 1 mm thick agarose pad made with the same medium, including DOC and αF, placed a coverslip on the pad and sealed the edges with Vaseline.

We imaged the cells on the same microscope used for recruitment assays. We used a 550-nm long-pass filter (Edmund Optics) in the transmitted light path to avoid photoexciting the LOV domain when using phase contrast. Once per minute we took a 1-s confocal image of mCherry fluorescence and a 100 ms confocal phase contrast image, and photoexcited the cells using the Micropoint laser. We used the same photoexcitation duration and intensity as for spot recruitment. For '– photoexcitation', the experiment was performed identically, except with the laser switched off.

A MetaMorph journal recorded the laser targets directly into a stack of phase contrast images. Using ImageJ, we made composites of the phase contrast and mCherry images, and measured the angle between the laser target and the incipient polarized growth. We binned the measured angles using Excel, and plotted the results using Igor Pro. We also performed a two-sample Kolmogorov-Smirnov test using Igor Pro.

We estimated the uncertainty in laser targeting to be 0.6–0.8 µm, and the corresponding angular uncertainty to be ~15° for a 5 µm yeast cell. This uncertainty limits the precision with which we can measure the angle between photoexcitation and polarized growth. Furthermore, this uncertainty is compounded by human error in updating targets in real time. Thus it is likely that the laser narrowly missed some cells during some photoexcitation cycles, although we do not know to what extent a near miss by the laser would photoexcite LOVpep.

We also note a slight tendency of polarization toward the mock photoexcitation target (**Fig. 3c**). To facilitate interpretation of the data, we avoided placing the laser target at points of cell-cell contact. This may have the unintended effect of biasing target placement toward the default polarization cue or away from regions of higher pheromone degradation.

31. Jansen, G., Wu, C., Schade, B., Thomas, D.Y. & Whiteway, M. Drag&Drop cloning in yeast. *Gene* **344**, 43–51 (2005).
32. Gietz, R.D. & Sugino, A. New yeast-*Escherichia coli* shuttle vectors constructed with in vitro mutagenized yeast genes lacking six-base pair restriction sites. *Gene* **74**, 527–534 (1988).
33. Janke, C. *et al.* A versatile toolbox for PCR-based tagging of yeast genes: new fluorescent proteins, more markers and promoter substitution cassettes. *Yeast* **21**, 947–962 (2004).
34. Gietz, R.D. & Woods, R.A. Transformation of yeast by lithium acetate/single-stranded carrier DNA/polyethylene glycol method. *Methods Enzymol.* **350**, 87–96 (2002).
35. Picard, D. Posttranslational regulation of proteins by fusions to steroid-binding domains. *Methods Enzymol.* **327**, 385–401 (2000).
36. Storici, F. & Resnick, M.A. The delitto perfetto approach to *in vivo* site-directed mutagenesis and chromosome rearrangements with synthetic oligonucleotides in yeast. *Methods Enzymol.* **409**, 329–345 (2006).
37. Longtine, M.S. *et al.* Additional modules for versatile and economical PCR-based gene deletion and modification in *Saccharomyces cerevisiae*. *Yeast* **14**, 953–961 (1998).
38. Gibson, D.G. *et al.* Enzymatic assembly of DNA molecules up to several hundred kilobases. *Nat. Methods* **6**, 343–345 (2009).
39. Thorn, K. Spinning-disk confocal microscopy of yeast. *Methods Enzymol.* **470**, 581–602 (2010).

40. Thevenaz, P., Ruttimann, U.E. & Unser, M. A pyramid approach to subpixel registration based on intensity. *IEEE Trans. Image Process.* **7**, 27–41 (1998).

41. Bodvard, K. *et al.* Continuous light exposure causes cumulative stress that affects the localization oscillation dynamics of the transcription factor Msn2p. *Biochim. Biophys. Acta* **1813**, 358–366 (2011).

doi:10.1038/nmeth.1904